
The fine line between dead neurons and sparsity in binarized spiking neural networks

Jason K. Eshraghian^{1,2} Wei D. Lu¹

Abstract

Spiking neural networks can compensate for quantization error by encoding information either in the temporal domain, or by processing discretized quantities in hidden states of higher precision. In theory, a wide dynamic range state-space enables multiple binarized inputs to be accumulated together, thus improving the representational capacity of individual neurons. This may be achieved by increasing the firing threshold, but make it too high and sparse spike activity turns into no spike emission. In this paper, we propose the use of ‘threshold annealing’ as a warm-up method for firing thresholds. We show it enables the propagation of spikes across multiple layers where neurons would otherwise cease to fire, and in doing so, achieve highly competitive results on four diverse datasets, despite using binarized weights. Source code is available at <https://github.com/jeshraghian/snn-tha/>.

1. Introduction

Memory access and data communication remain amongst the most expensive instructions in deep learning workloads (Hashemi et al., 2018; Kozyrakis et al., 2010). To complement Feynman¹, there is plenty of room for optimization at the top of the stack: learning algorithms can be tweaked to decrease memory access frequency using activation sparsity, and to reduce memory usage by weight quantization.

Activation sparsity: spiking neural networks (SNNs) are an example of models that leverage activation sparsity $z \in \{0, 1\}^n$, where an activation $z^i = 0$ allows input-weight-multiply steps to be bypassed as the product is guar-

anteed to also return ‘0’. Memory access to read out weights can be skipped (Roy et al., 2019; Eshraghian et al., 2021).

Reduced weight precision: parameter quantization directly reduces the number of memory cells that must be read at any compute cycle. In the extreme, binarized neural networks (BNNs) constrain each weight to $w^{ij} \in \{-1, 1\}$ at the cost of reduced representational capacity and challenging learning convergence (Hubara et al., 2016; Courbariaux et al., 2016).

SNNs can amortize the cost of binarization by: 1) distributing information in the temporal domain rather than the activation amplitude (Voelker et al., 2020; Kheradpisheh et al., 2021), and 2) accumulating binarized data in the high-precision, dynamically evolving state-space of spiking neurons (Schaefer & Joshi, 2020; Laborieux et al., 2021). In both cases, discrete activations are applied to a continuous domain (either time or neuron state).

The dynamic range of the neuron state can be increased by using a large firing threshold. This is crucial for binarized SNNs (BSNNs), as it extends the range over which discrete inputs may be accumulated. However, indefinitely increasing the threshold impedes neuronal activity (and therefore, learning), leading to the ‘dead neuron problem’. To offset this issue, we propose ‘threshold annealing’, a warm-up technique that improves classification accuracy in supervised learning tasks across four datasets (two static, two dynamic). This is achieved by dynamically increasing the threshold outside of the training-loop which enables:

- *early* epochs to achieve sufficient network activity for low-precision learning to take place (i.e., by using a small threshold to promote adequate neuronal firing),
- *later* epochs to utilize the wide dynamic range state-space of spiking neurons for fine-tuning at increased precision (i.e., large thresholds that enable accumulation of multiple binarized quantities).

Our findings show state-of-the-art performance on all four datasets when compared to similarly lightweight networks, and a reduction of dead neurons on the most challenging dataset by 71% when compared to BSNNs without threshold annealing, leading to faster training convergence.

¹Department of Electrical Engineering and Computer Science, University of Michigan, MI, USA ²Department of Computer Science and Software Engineering, University of Western Australia, WA, Australia. Correspondence to: Jason K. Eshraghian <jasonesh@umich.edu>, Wei D. Lu <wluee@umich.edu>.

¹And his American Physical Society lecture titled ‘There is Plenty of Room at the Bottom’ (Feynman, 1959).

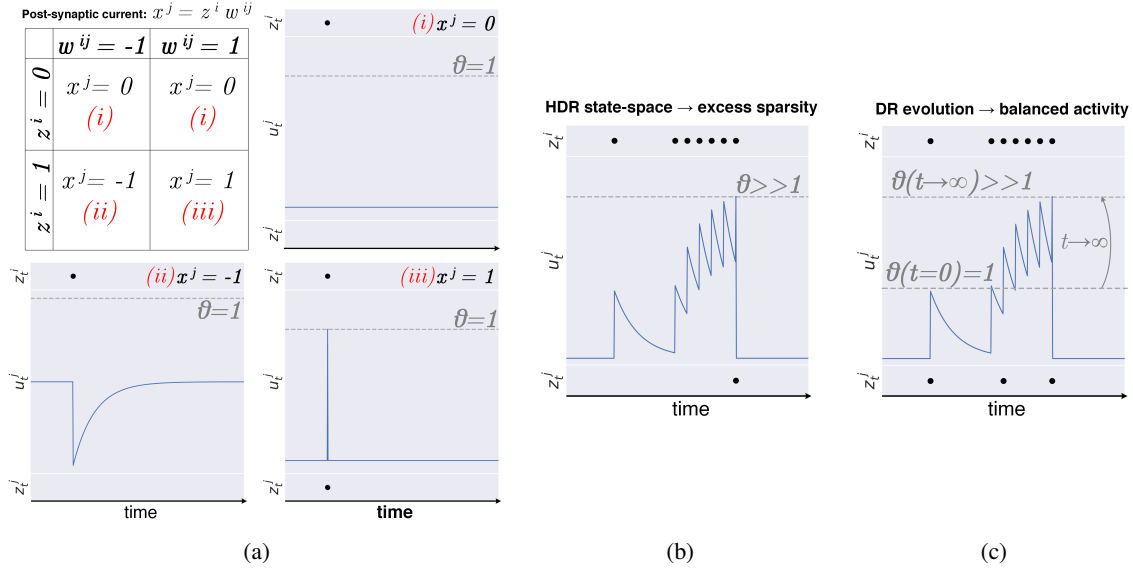


Figure 1. (a) Neuron response to the three possible post-synaptic currents x^j : (i) $x^j = 0$: No response if $w^{ij} = 0$, (ii) $x^j = -1$: Negative deflection with short-term memory but no spiking activity, (iii) $x^j = +1$: Spike propagation but no short-term memory due to reset. (b) High dynamic range (HDR) state precision comes at the expense of suppressed network activity. (c) Gradual evolution of the dynamic range (DR) balances precision and spike emission. Threshold annealing follows a similar principle, but the threshold θ is increased over training iterations instead of time. Spiking neuron parameters are thus fixed at run time, reducing computation and memory costs.

2. Background

2.1. Spiking Neuron Model

SNNs adopt the same topologies modeled by conventional neural networks, but with the artificial neuron traded for a spiking neuron model. A single-state leaky integrate-and-fire neuron derived using the forward Euler method (Appendix A) governed by the following discrete-time dynamics is used (Lapique, 1907; Gerstner & Kistler, 2002):

$$u_{t+1}^j = \beta u_t^j + \sum_i w^{ij} z_{t+1}^i - z_t^j \theta, \quad (1)$$

$$z_t^j = \begin{cases} 1, & \text{if } u_t^j \geq \theta \\ 0, & \text{otherwise,} \end{cases} \quad (2)$$

where u_t^j is the hidden state (membrane potential) of neuron j at time t ; β is the decay rate of membrane potential; w^{ij} is the weight between neurons i and j ; and a spike z_t^j is elicited if the potential exceeds the threshold θ . The final term of Equation (1) resets the state by subtracting the threshold θ each time an output spike is generated.

2.2. Binarized SNNs

In BSNNs, each input spike $z_{t+1}^i \in \{0, 1\}$ is scaled by a binarized weight $w^{ij} \in \{-1, 1\}$, resulting in a trinary post-synaptic potential $x_{t+1}^j = w^{ij} z_{t+1}^i \in \{-1, 0, 1\}$. This is

added to the hidden state of a downstream neuron u_t^j , which triggers its own spike given sufficient excitation $u_t^j \geq \theta$. With threshold normalization,² the three possible outcomes while the membrane potential is at rest are depicted in Figure 1(a). In case (i), a nulled activation means no state change. In case (ii), the neuron is inhibited and the hidden state follows a continuous trajectory back to its resting value. This is the only case where memory dynamics persist. In case (iii), the state immediately reaches the firing threshold $u^j = \theta$ upon spike arrival, and is subsequently forced to reset $u^j \leftarrow 0$. This is the only case where information is propagated to deeper layers. A problem emerges: short-term memory and spike emission are mutually exclusive.

Using a large threshold is the most obvious solution (Lu & Sengupta, 2020), and achieves several benefits illustrated in Figure 1(b):

- the dynamic range of the state-space is increased,
- multiple inputs may be accumulated, and
- excitatory inputs can now be sustained as short-term, recurrent memory.

But these benefits do not indefinitely hold - too high a thresh-

²Normalizing $\theta = 1$ is common practice as it both enables the surrogate gradient term $\partial z^j / \partial u^j$ to be interpreted as a firing probability (Shrestha & Orchard, 2018; Zenke & Vogels, 2021), and is also simple (Booij & Nguyen, 2005).

old obstructs the state from ever reaching it, causing spiking sparsity to extinguish into dead neurons. Large thresholds also increase susceptibility to vanishing gradients from an effect that is independent of dead neurons; surrogate gradients are typical activation functions (e.g., sigmoid, tanh, fast-sigmoid) centered about the firing threshold. Shift the surrogate function too far, and many neurons will dominantly operate in the subthreshold regime where $\partial z^i / \partial u^i \rightarrow 0$.

Another drawback of using large thresholds is that it may interfere with gradient-based methods that rely on low thresholds to promote more neuronal activity, which is often the case for spike-time derivative methods and single-spike training schemes (Bohte et al., 2002; Boojj & tat Nguyen, 2005; Xu et al., 2013). These conflicting trade-offs must somehow be balanced.

2.3. Related Work

Inspired by mechanisms that promote stability in the primary sensory cortex, threshold adaptation has been incorporated into computational models of synaptic plasticity (Bienenstock et al., 1982; Zhang & Linden, 2003). Adaptation has been used as a homeostatic mechanism to regulate network activity in deep learning-inspired SNNs trained via local learning rules (Diehl & Cook, 2015) and gradient-based optimization (Bellec et al., 2018; Shaban et al., 2021). In all previous cases, threshold adaptation evolves over the course of simulated time steps (Figure 1(c)). It has shown to be a potential approach to retaining long-term memory dynamics in SNNs using biologically plausible means, with the cost of each neuron updating its threshold trajectory at each time step. While this scales memory complexity linearly with the number of neurons $\mathcal{O}(n)$ during the forward-pass, the threshold must be recorded at every time step during training to implement the backpropagation (BPTT) algorithm, which additionally scales memory usage with time as well $\mathcal{O}(nT)$ (Rumelhart et al., 1986; Werbos, 1990). This is overhead that we aim to eliminate in a compute and memory bound system, such as a BSNN, by i) moving the threshold evolution outside of the weight update loop, and ii) using a shared threshold for each layer.

By eliminating the temporal variation of the threshold (i.e., it is only varied between training iterations), the purposes of membrane potential and threshold can be better decoupled. The membrane potential can be thought of as the mechanism for temporal data retention, while threshold warm-up leads to an evolving dynamic range state-space which enables inter-layer spike propagation.

3. Threshold Annealing

Out-of-the-loop threshold updates reduces complexity: See Algorithm 1 for pseudo-code of our proposed *thresh-*

Algorithm 1 Threshold Annealing

Require: $\theta_0 \in \mathbb{R}_{>0}$: Initial threshold
Require: $\theta_\infty \in \mathbb{R}_{>\theta_0}$: Final threshold
Require: $\alpha\theta \in \mathbb{R}_{>0}$: Inverse threshold time constant
Require: w : Initial parameters
Require: η : Learning rate
 $\theta_\gamma \leftarrow \theta_0$ (Initialize threshold)
 $s \leftarrow \partial \tilde{z}(\theta_0) / \partial u$ (Initialize surrogate gradient using θ_0)
 $\gamma \leftarrow 0$ (Initialize training step)
while w not converged **do**
 $\gamma \leftarrow \gamma + 1$
 $g_\gamma \leftarrow \nabla_w f_\gamma(s, w_{\gamma-1})$ (Get gradients w.r.t. surrogate gradient s using initial threshold θ_0)
 $w_\gamma \leftarrow w_{\gamma-1} - \eta \cdot g_\gamma$ (Update parameters e.g. using SGD or Adam)
 $\theta_\gamma \leftarrow \theta_{\gamma-1} + \alpha(\theta_\infty - \theta_{\gamma-1})$ (Update threshold without updating s)
end while
return: w_γ (Resulting parameters)

old annealing method. Appendix B provides more detailed pseudo-code that highlights how temporal evolution is isolated from spiking dynamics. A neuron’s firing threshold exponentially relaxes from an initial value θ_0 to a larger final value θ_∞ with time constant τ_θ :

$$\tau_\theta \frac{d\theta_\gamma}{d\gamma} = -\theta_\gamma + \theta_\infty, \quad \theta_\infty > \theta_\gamma \quad (3)$$

where all neurons in each layer share the following explicit update rule at each training iteration γ :

$$\theta_{\gamma+1} = \theta_\gamma + \alpha(\theta_\infty - \theta_\gamma) \quad (4)$$

and $\alpha = \exp(-1/\tau_\theta)$ is the inverse time constant of the threshold, noting that time here refers to the span of training iterations rather than the temporal dynamics of a spiking neuron. By only updating the threshold outside of the temporal evolution of each forward-pass (i.e., θ_γ is fixed during inference), memory no longer scales with time, and it also does not scale with iterations γ as the BPTT algorithm truncates the computational graph between iterations. For shared thresholds per layer, memory scales with $\mathcal{O}(L) \ll \mathcal{O}(nT)$, where L is the number of layers in the network.

Fast to slow evolution balances weight updates with threshold updates: The threshold dynamics are designed to follow the evolution of the effective learning rate. For example, when using the Adam optimizer, the estimation of moments (and therefore, weight updates) exponentially decays over iterations (Kingma & Ba, 2014). Aligning the rate of threshold and weight updates is desirable as it avoids either of the two having an overpowering effect on

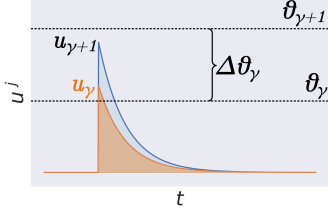


Figure 2. Membrane potential u^j changes across iterations as a function of weight updates. If the threshold update across training iterations $\Delta\theta_\gamma$ is greater than the change of membrane potential, then a spike from iteration γ will no longer occur at $\gamma+1$. Imposing the constraint from Equation (5) prevents this. Note: the reset mechanism is not depicted for visual clarity.

the network: excessively large threshold updates will clip too many spikes at the start of training (similarly to Figure 1(b)), whereas exceedingly small threshold updates fails to sufficiently extend the dynamic range of the state-space (the problems depicted in Figure 1(a)).

To ensure that a threshold update does not lead to the elimination of any spikes whilst still expanding the state-space of a neuron, the threshold change $\Delta\theta_\gamma = \theta_{\gamma+1} - \theta_\gamma$ should be bounded by the distance between the new membrane potential at iteration $\gamma + 1$ from the original threshold at γ :

$$\Delta\theta_\gamma < u_{\gamma+1} - \theta_\gamma \quad (5)$$

This is visually depicted in Figure 2, where neglecting the condition from Equation (5) would suppress spikes. If this condition is neglected for all of time t , the neuron would cease to contribute to the loss function, and lack a gradient signal to contribute to learning, i.e., a dead neuron. From the derivation provided in Appendix C, the following two constraints can be imposed on θ_γ and θ_∞ to prevent threshold annealing from contributing to dead neurons:

$$(1 - \alpha)\theta_\gamma + \alpha\theta_\infty < \mathbf{z} \cdot \left(\mathbf{w}_\gamma^{::j} + \eta \frac{\partial \mathcal{L}}{\partial \mathbf{w}_\gamma^{::j}} \right) \quad (6)$$

$$\theta_\infty < \mathbf{z} \cdot \mathbf{w}_\infty^{::j} \quad (7)$$

where $\mathbf{z} \in \mathbb{R}^i$ is the input vector, and $\mathbf{w}_\gamma^{::j} \in \mathbb{R}^i$ is the weight vector connected to the j^{th} neuron of the first layer, and $\mathbf{w}_\infty^{::j}$ is the final weight vector at the end of training.

The weight update term on the right-hand side of Equation (6) assumes stochastic gradient descent (SGD) is used, where for adaptive optimizers the derivative term often decays exponentially with network converges. As θ_∞ is a constant term, the evolution of θ_γ should also exponentially

diminish. This is adhered to in Equation (4), and balances the two objectives of i) using a large threshold, while ii) not inducing dead neurons due to threshold updates.

More intuitively, during early training iterations, the weight updates are large enough to ‘catch up’ to the effect of a large threshold step. This is because the effect of weight decay is minimal during early training iterations. As the network is trained for more epochs, threshold updates are reduced to match that of weight decay.

In the experiments that follow, we adhere to exponential decay of threshold update magnitude as per Equation (4) and choose θ_∞ , θ_γ and α based on a hyperparameter search. For sparsely populated input data, i.e., where the mean of the input features \mathbf{z} over time is quite small (e.g., the Spiking Heidelberg Digits dataset (Cramer et al., 2020)), the optimal value of α reduces by several orders of magnitude to slow down the rate at which θ_γ converges to θ_∞ (see Appendix D.3). This result is independently predicted by Equation (6).

Clamped surrogate gradients boost the weight update signal for subthreshold neurons:

The conventional method to account for the non-differentiability of Equation (2) is to use a surrogate gradient which substitutes the Heaviside operator with a threshold-shifted, differentiable alternative e.g., the sigmoid function, in the backward pass (see Figure 3). If this approach was strictly adhered to, then the surrogate function would shift along with the threshold over training iterations.

Consider a neuron with a subthreshold membrane potential at point A, depicted in Figure 3. Shifting the surrogate function along with the threshold causes $s_t^j \rightarrow 0$, i.e., the vanishing gradient problem (contrasted from the dead neuron problem, where neurons cease to fire).

To address this issue, our implementation clamps the surrogate gradient to the initial threshold value θ_0 , preventing the function from shifting during the training process. This is highlighted in Algorithm 1, where the threshold θ_γ is updated without updating the surrogate gradient s . Our experiments use the fast sigmoid function:

$$s_t^j = \frac{\partial z_t^j}{\partial u_t^j} \leftarrow \frac{1}{(1 + k|\theta_0 - u_t^j|)^2} \quad (8)$$

where the left arrow denotes substitution, and k is a slope that modulates the linearity of the surrogate function. While the learning process is generally robust to the choice of the surrogate gradient (Zenke & Vogels, 2021), we choose to fix the gradient based on the initial threshold θ_0 as it removes the need to re-compute a new surrogate function at each iteration.

The primary benefit is that the gradient signal is boosted for

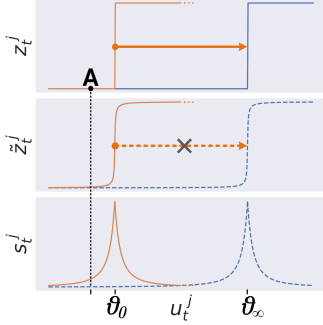


Figure 3. **Top row:** output spiking activity z_t^j is represented with the Heaviside operator centered about the firing threshold. Over iterations, threshold annealing pushes the Heaviside operator along the x-axis. **Middle row:** Surrogate of the Heaviside operator to address non-differentiability \tilde{z}_t^j . Our approach does not shift the surrogate function which reduces the impact of vanishing gradients on subthreshold neurons (e.g., at point A). **Bottom row:** the surrogate gradient s_t^j . The intersection between a neuron at point A and the non-shifted gradient is larger than that of the shifted gradient, thus providing latent/quiet neurons with the opportunity to continue learning, and therefore contribute to network activity.

neurons closer to their resting potential. Quantitatively, for a neuron at rest $u_t^j \approx 0$ and $\theta \gg 1$, and assuming $k = 1$, then $s_t^j \approx 1/\theta^2$ (based on Equation (8)). In practice, θ_∞ can be close to one order of magnitude larger than θ_0 (see Appendix D.1 and Appendix D.3 for examples). If θ_γ is used in Equation (8) instead, this would reduce s_t^j (and by extension, $\nabla_w \mathcal{L}$) by the square of this factor as $\theta_\gamma \rightarrow \theta_\infty$.

This benefit does not come for free, as active neurons in later training iterations (where $u_t^j \approx \theta_\infty$) face the same problem of a vanishing s_t^j . We claim this is tolerable for two empirical reasons: i) upon spike emission, the membrane potential of an active neuron is reset where a low u^j provides an opportunity for the neuron to learn at another time step, and ii) the neuron must have already been trained in earlier iterations for its membrane potential to reach a large value θ_∞ (see Figure 4(d) for an experiment where u^j starts at rest and is trained to approach $\theta_\infty = 50$). Quiet neurons are therefore provided with a better opportunity to contribute to network activity via gradient clamping.

4. Experimental Results

We test a full precision SNN and several BSNNs under the following cases i) with a normalized threshold $\theta = 1$, ii) with a fixed threshold determined by a hyperparameter search, and iii) using threshold annealing, for each experiment on four datasets ranging from simple to increasingly difficult: MNIST (LeCun et al., 1998), FashionMNIST

(Xiao et al., 2017), DVS128 Gesture (Amir et al., 2017), and Spiking Heidelberg Digits (SHD) (Cramer et al., 2020), without dataset augmentation. All experiments were performed on a 16GB NVIDIA V100 GPU, conducted across 5 trials each. Hyperparameters were selected based on a sweep over 500 trials for each individual experiments (see Appendix D for further details). We used snnTorch 0.4.11 to construct spiking neuron models (Eshraghian et al., 2021) which uses a PyTorch 1.10.1 backend (Paszke et al., 2019) in Python 3.7.9.

4.1. Temporal Coding

Before moving to more complex data-driven tasks, we first provide an interpretable demonstration of how threshold annealing can improve BSNN performance on a straightforward spike-time encoding task. A single output neuron is trained to fire at a target time step by encouraging the membrane potential to linearly increase to the threshold at $t = 75$, and subsequently remain quiet upon spike emission. A 3-layer BSNN is used with a fully-connected architecture of 100-1000-1 neurons. The input to the network is a Poisson spike train simulated across 100 time steps. The mean square error between the target and actual membrane potential are summed at each time step. Precise implementation details are provided in Appendix D.1.

Figure 4 depicts the membrane potential trace of the output neuron over time at several training iterations γ . The full precision network in (a) accomplishes the task with ease, while the BSNN with $\theta = 1$ in (b) highlights the challenges described in Section 2.2, i.e., the neuron is unable to both emit spikes as well as retain memory. Increasing the threshold of all neurons to $\theta = 50$ completely suppresses spiking activity in the hidden and output layers. The membrane potential increases due to the bias, and settles at approximately the midpoint between steady-state and threshold, where the loss of the triangular membrane potential target is minimized. To fix the memory leakage problem in (b) and the dead neuron problem in (c), threshold annealing is applied by gradually warming up $\theta_0 = 5$ to $\theta_\infty = 50$ with an inverse threshold time constant $\alpha = 5 \times 10^{-3}$ (Equation (4)). The low threshold at the first iteration $\gamma = 0$ enables spike propagation throughout layers, which sustains sufficient activity to keep the network learning over epochs. At the 400th iteration, the BSNN with threshold annealing successfully emits a spike at the target time step. The output neuron continued to remain active at the end of the simulation, where θ_γ was within 0.1% of the θ_∞ ; a definitive improvement over use of a fixed threshold in Figure 4(c). Animations in the source code offer further visual intuition on how threshold annealing ‘pulls up’ neuronal activity.

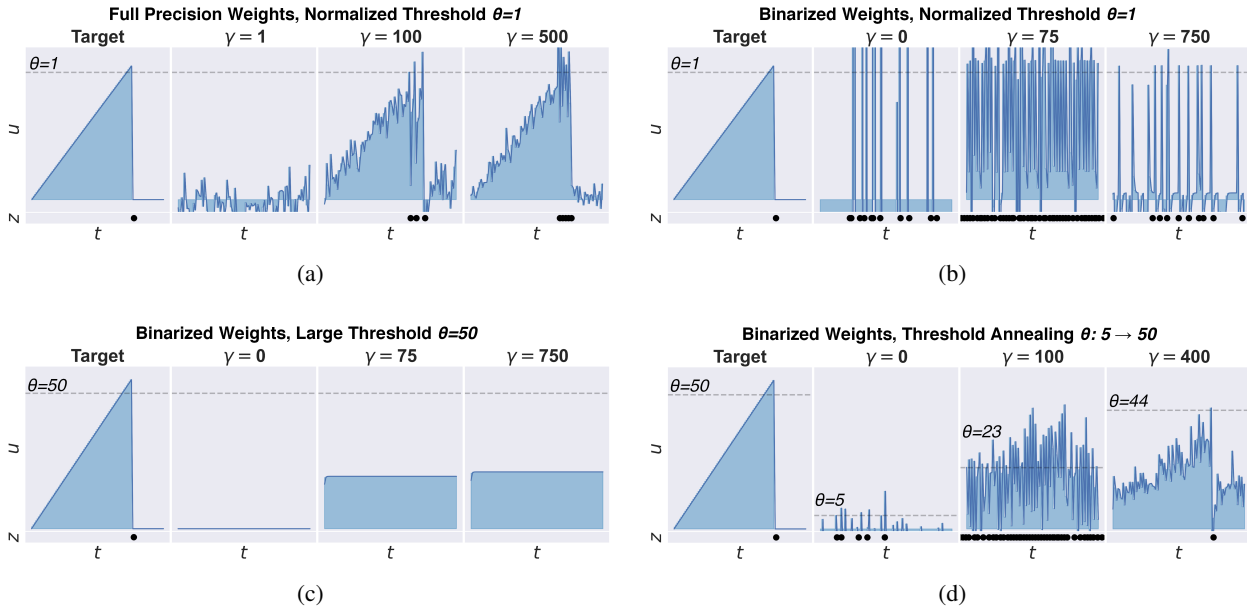


Figure 4. An intuitive demonstration of threshold annealing on a spike timing task. (a) Full precision weights with threshold $\theta = 1$. (b) Binarized weights with threshold $\theta = 1$ leads to unstable neuronal activity. (c) Binarized weights with a large threshold $\theta = 50$ suppresses all firing activity; the increase in hidden state u is due to an increasing bias. (d) Binarized weights with threshold annealing from $\theta : 5 \rightarrow 50$ successfully learns to fire at the desired spike-time at the 400th iteration. The performance better matches that of the full precision network. Animated visualizations are provided at the following link: github.com/jeshraghian/snn-tha/.

4.2. Static Datasets

The MNIST (LeCun et al., 1998) and the slightly more challenging FashionMNIST datasets (Xiao et al., 2017) are used to assess the performance of threshold annealing on temporally static data. Both datasets consist of 60,000 28×28 greyscale images in the training set, and 10,000 images in the test set, with 10 output classes of handwritten digits (MNIST) and clothing items/accessories (FashionMNIST). The convolutional BSNN architecture is provided in the Table 1 footnote: 16Conv5 refers to a 5×5 convolutional kernel with 16 filters; AP2 is a 2×2 average-pooling layer applied to membrane potential, and 1024Dense10 is a dense layer with 1024 inputs and 10 outputs.

The raw datasets are passed to the BSNN for 100 time steps of simulation without input encoding. The predicted class is set to the neuron with the highest spike count at the end of the 100 time steps. Hyperparameters and the optimization process for each experiment are provided in Appendix D.2, and the final results are shown in Table 1, where our proposed threshold annealing technique improves the performance of BSNNs by an average of 0.3% for MNIST, and 0.97% for FashionMNIST over the next best BSNN. The worst-case scenario of a BSNN with a normalized threshold still performs reasonably well, on account of static datasets not requiring any memory retention. Performance degrades further when temporal dynamics are included.

Table 1. Test set accuracies for static datasets.

	MNIST			FashionMNIST		
	Best	Mean	σ	Best	Mean	σ
flt32	99.45	99.31	0.12	91.13	91.03	0.09
BSNN, $\theta:1$	98.46	98.44	0.02	87.11	86.70	0.36
BSNN	98.81	98.77	0.06	87.01	86.95	0.10
Proposed	99.12	99.07	0.04	88.12	87.92	0.22

¹ 16Conv5-AP2-64Conv5-AP2-1024Dense10.

² σ : Sample standard deviation.

4.3. Temporal Datasets

The DVS128 Gesture dataset (Amir et al., 2017) is filmed with an event-based camera (Patrick et al., 2008) which only processes sufficient changes in luminance, and consists of 11 different output classes of hand gestures, such as clapping, arm rotation, and air guitar. To fit the dataset within 100 time steps, events were integrated over a period of 5 ms such that each sample in the training and test set are approximately 1 s and 3.5 s in duration, respectively. Spatial downsampling fits each sample to dimensions of $(2 \times 32 \times 32)$.

As a more challenging alternative, the SHD dataset was also used which consists of 20 output classes of audio record-

Table 2. Test set accuracies for temporal datasets.

	DVS128 Gesture			SHD		
	Best	Mean	σ	Best	Mean	σ
flt32	93.05	92.87	0.32	82.51	82.27	0.27
BSNN, θ :1	84.37	84.03	0.60	63.86	62.99	0.91
BSNN	89.24	88.54	0.70	62.94	62.48	0.41
Proposed	92.36	91.32	0.56	66.35	65.68	0.66

¹ DVS128: 16Conv5-AP2-32Conv5-AP2-8800Dense11.

² SHD: 700Dense3000Dense20.

³ σ : Sample standard deviation.

ings of the ten digits spoken aloud in both the English and German languages. The recordings are processed using a cochlear model for spike encoding (Cramer *et al.*, 2020).

The final test accuracies are shown in Table 2, with experimental and hyperparameter details in Appendix D.3. As dataset complexity increases, the performance of BSNNs degrade further, while threshold annealing offsets the degradation to a larger degree. For the DVS128 Gesture dataset, when compared to the full precision network, the baseline BSNNs with and without threshold normalization drop by 8.8% and 4.4%, respectively. But this performance drop is reduced significantly to 1.5% when threshold annealing is used during training. These results indicate that BSNNs have an optimal solution that does not deviate far from the high precision case; the challenge is finding this solution. Methods such as threshold annealing make the training process easier.

Performance drops drastically for the SHD dataset when binarizing weights across all cases. While threshold annealing improves upon performance by 2.7% compared to the next best BSNN, it still remains at a large distance from the high precision performance. While this may partially be accounted for by complexity of the SHD dataset, it may also be due to the additional hyperparameters that are introduced which require a larger number of trials during the hyperparameter search process. For fairness, the number of random trials was set to 500 for all networks, though threshold annealing would likely benefit from increasing the search space.

5. Discussion

5.1. Comparison with lightweight SNNs

There is a general lack of reproducible baselines that implement gradient-based learning on convolutional BSNNs, likely due to hyperparameter sensitivity and the associated difficulty in training. The few related approaches in-

clude Lu and Sengupta’s ANN-SNN conversion which is benchmarked on large-scale static datasets (Lu & Sengupta, 2020). Kheradpisheh *et al.* use temporal backpropagation (BS4NN) on dense BSNNs (Kheradpisheh *et al.*, 2021). We further consider several additional promising lightweight approaches to training full precision SNNs, including sparse spiking gradient descent (SSGD) which reduces overhead during gradient calculations (Perez-Nieves & Goodman, 2021), and neural heterogeneity (NH) which compresses the required number of neurons with the addition of neuron-independent parameters (Perez-Nieves *et al.*, 2021). Interestingly, BSNNs with threshold annealing can outperform full precision SNNs in terms of accuracy using considerably less memory for model parameters. These baselines rely on dense networks only, which is why we developed our own full precision and BSNN baselines in previous sections.

FashionMNIST: SSGD and NH achieve 86.7% and 87.5%, respectively, using full precision weights. NH requires 101k full precision weights (3.2 Mbits). BS4NN achieves 87.3% using 794 Kbits of binarized parameters. Threshold annealing outperforms in terms of accuracy at 87.9% with far less memory footprint with 12k binarized weights (12 Kbits).

DVS128 Gesture: NH obtains 82.1%, whereas our BSNN approach obtains 91.3% with less memory overhead. Assuming the input dimensions of the DVS128 Gesture dataset are downsampled by a factor of 4, the network in NH requires 8.4 Mbits of full precision weights as against 98 Kbits of binarized weights in our approach.

SHD: In contrast to the above results, both full precision NH (82.7%) and SSGD (77.5%) outperform our BSNN (65.7%). This can be attributed to the use of recurrent connections in NH and SSGD; without recurrent SNNs in SSGD, performance dropped below 50%. Likewise from Cramer *et al.*’s original proposal of the SHD dataset, the test accuracy was 48.6% on a similarly 2-layer dense network (Cramer *et al.*, 2020), which our BSNN with threshold annealing outperforms by around 17%. When recurrent connections were added, test accuracy jumped to 83.2%. Although we use a considerably wider hidden layer (3000 neurons vs 128 neurons in NH), binarized weights still occupy less memory (ours: 2.16 Mbits vs NH: 2.95 Mbits).

5.2. Spiking Activity and Convergence Rate

Figure 5 shows the distribution of spiking activity across layers both with and without threshold annealing. This is measured by passing the entire test set to the network and taking the average spike count for each neuron. For the fixed threshold network trained on the SHD dataset, 55% and 90% of neurons in the first and final layer do not contribute to network activity, compared to approximately 20% with threshold annealing in both layers. This is highly undesirable at the start of the learning process as gradients

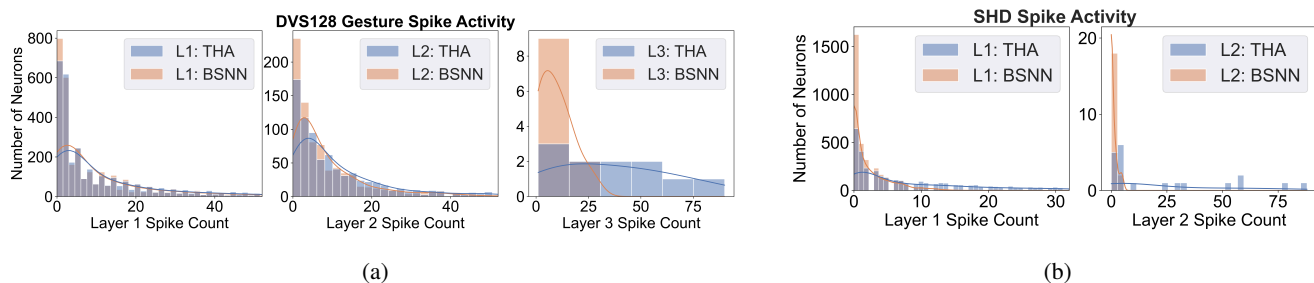


Figure 5. Spiking activity across layers with threshold annealing (THA) and without (BSNN) on temporal datasets. Static dataset distributions are provided in Appendix E.1. (a) **DVS128 Gesture**: Distribution of spikes in the output layer with threshold annealing is balanced, whereas most neurons are silent without annealing. (c) **SHD**: Using a dataset with sparse activity results in a large number of dead without threshold annealing.

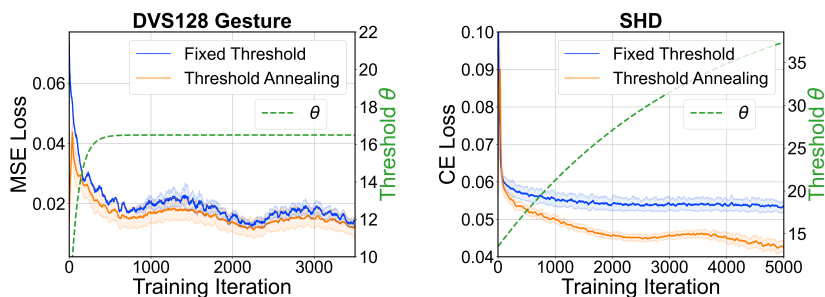


Figure 6. Loss curves on dynamic datasets. Oscillations are a result of using periodic learning rate schedule.

cannot backpropagate through neurons that do not contribute to the final loss, which causes slower training convergence. This is shown in Figure 6, where the larger proportion of dead neurons in the fixed threshold network trained on the SHD dataset leads to worse performance. Averaging across both layers, threshold annealing reduces the number of dead neurons by 71% in the SHD network.

The threshold dynamics of the final layer of both networks are also overlaid, where the rate of increase is slower when trained on SHD than DVS128 Gesture. This is a result of sparser input activity, and was predicted by Equation (7). Once the training process is terminated based on early stopping criteria, the same thresholds of the optimal trial should be used. In all experiments, the final threshold θ_γ was always within 0.1% of the steady-state threshold θ_∞ , so we simply use θ_∞ at test time.

5.3. Concluding remarks

In general, our approach to training BSNNs is extremely competitive when compared to high precision, lightweight networks that consume more memory. As our implementation is based on a PyTorch backend, the binarized weights are represented as full precision values and are not explicitly

stored with compressed memory. Rather, the models generated are intended to be ported onto dedicated neuromorphic hardware that is tailored for single-bit weight representations (Orchard et al., 2021; Akbarzadeh-Sherbaf et al., 2020; Rahimi Azghadi et al., 2020).

It is also important to account for how this memory is used. For example, while the memory overhead of synaptic weights scale with the number of neurons as $\mathcal{O}(n^2)$, SNNs in general are power efficient as this memory can be accessed with low frequency. On the other hand, neuron specific parameters, such as in neural heterogeneity (Perez-Nieves et al., 2021) and threshold adaptation (Bellec et al., 2018), have less memory complexity $\mathcal{O}(n)$, but this memory must be accessed at each time step to update the hidden state and does not benefit from spike sparsity. By sharing thresholds for neurons in given layers, threshold annealing not only adds negligible memory footprint (i.e., one full precision value per layer), but it does so with good performance. Combining threshold annealing with heterogeneous time constants and recurrent connections could attract the benefits of both worlds in lightweight BSNN computation, especially where intrinsic circuit-level variations can be exploited as diverse neuronal behavior (Kang et al., 2021).

Acknowledgements

This work was supported, in part, by the Semiconductor Research Corporation and DARPA, through the Applications Driving Architectures Research Center, and the National Science Foundation through awards ECCS-191550 and CCF-1900675. Jason K. Eshraghian is supported by the Forrest Research Fellowship through the Forrest Research Foundation.

References

- Akbarzadeh-Sherbaf, K., Safari, S., and Vahabie, A.-H. A digital hardware implementation of spiking neural networks with binary FORCE training. *Neurocomputing*, 412:129–142, 2020.
- Akiba, T., Sano, S., Yanase, T., Ohta, T., and Koyama, M. Optuna: A next-generation hyperparameter optimization framework. In *Proceedings of the 25th ACM SIGKDD International Conference on Knowledge Discovery & Data Mining*, pp. 2623–2631, 2019.
- Amir, A. et al. A low power, fully event-based gesture recognition system. In *Proceedings of the IEEE Conference on Computer Vision and Pattern Recognition*, pp. 7243–7252, 2017.
- Azghadi, M. R., Lammie, C., Eshraghian, J. K., Payvand, M., Donati, E., Linares-Barranco, B., and Indiveri, G. Hardware implementation of deep network accelerators towards healthcare and biomedical applications. *IEEE Transactions on Biomedical Circuits and Systems*, 14(6): 1138–1159, 2020.
- Bellec, G., Salaj, D., Subramoney, A., Legenstein, R., and Maass, W. Long short-term memory and learning-to-learn in networks of spiking neurons. In *Proceedings of the 32nd International Conference on Neural Information Processing Systems*, pp. 795–805, 2018.
- Bergstra, J., Bardenet, R., Bengio, Y., and Kégl, B. Algorithms for hyper-parameter optimization. *Advances in Neural Information Processing Systems*, 24, 2011.
- Bienenstock, E. L., Cooper, L. N., and Munro, P. W. Theory for the development of neuron selectivity: orientation specificity and binocular interaction in visual cortex. *Journal of Neuroscience*, 2(1):32–48, 1982.
- Bohte, S. M., Kok, J. N., and La Poutre, H. Error-backpropagation in temporally encoded networks of spiking neurons. *Neurocomputing*, 48(1-4):17–37, 2002.
- Booij, O. and tat Nguyen, H. A gradient descent rule for spiking neurons emitting multiple spikes. *Information Processing Letters*, 95(6):552–558, 2005.
- Courbariaux, M., Hubara, I., Soudry, D., El-Yaniv, R., and Bengio, Y. Binarized neural networks: Training deep neural networks with weights and activations constrained to +1 or -1. *arXiv preprint arXiv:1602.02830*, 2016.
- Cramer, B., Stradmann, Y., Schemmel, J., and Zenke, F. The Heidelberg spiking data sets for the systematic evaluation of spiking neural networks. *IEEE Transactions on Neural Networks and Learning Systems*, 2020.
- Diehl, P. U. and Cook, M. Unsupervised learning of digit recognition using spike-timing-dependent plasticity. *Frontiers in Computational Neuroscience*, 9:99, 2015.
- Eshraghian, J. K., Ward, M., Neftci, E., Wang, X., Lenz, G., Dwivedi, G., Bennamoun, M., Jeong, D. S., and Lu, W. D. Training spiking neural networks using lessons from deep learning. *arXiv preprint arXiv:2109.12894*, 2021.
- Feynman, R. P. Plenty of room at the bottom. In *APS Annual Meeting*, 1959.
- Gerstner, W. and Kistler, W. M. *Spiking neuron models: Single neurons, populations, plasticity*. Cambridge University Press, 2002.
- Hashemi, M., Swersky, K., Smith, J., Ayers, G., Litz, H., Chang, J., Kozyrakis, C., and Ranganathan, P. Learning memory access patterns. In *International Conference on Machine Learning*, pp. 1919–1928. PMLR, 2018.
- He, T., Zhang, Z., Zhang, H., Zhang, Z., Xie, J., and Li, M. Bag of tricks for image classification with convolutional neural networks. In *Proceedings of the IEEE/CVF Conference on Computer Vision and Pattern Recognition*, pp. 558–567, 2019.
- Hubara, I., Courbariaux, M., Soudry, D., El-Yaniv, R., and Bengio, Y. Binarized neural networks. *Advances in Neural Information Processing Systems*, 29, 2016.
- Kang, S. M., Choi, D., Eshraghian, J. K., Zhou, P., Kim, J., Kong, B.-S., Zhu, X., Demirkol, A. S., Ascoli, A., Tetzlaff, R., et al. How to build a memristive integrate-and-fire model for spiking neuronal signal generation. *IEEE Transactions on Circuits and Systems I: Regular Papers*, 68(12):4837–4850, 2021.
- Kheradpisheh, S. R., Mirsadeghi, M., and Masquelier, T. BS4NN: Binarized spiking neural networks with temporal coding and learning. *Neural Processing Letters*, pp. 1–19, 2021.
- Kingma, D. P. and Ba, J. Adam: A method for stochastic optimization. *arXiv preprint arXiv:1412.6980*, 2014.
- Kozyrakis, C., Kansal, A., Sankar, S., and Vaid, K. Server engineering insights for large-scale online services. *IEEE Micro*, 30(4):8–19, 2010.

- Laborieux, A., Ernoult, M., Hirtzlin, T., and Querlioz, D. Synaptic metaplasticity in binarized neural networks. *Nature Communications*, 12(1):1–12, 2021.
- Lapique, L. Recherches quantitatives sur l’excitation électrique des nerfs traitée comme une polarisation. *Journal of Physiology and Pathology*, 9:620–635, 1907.
- LeCun, Y., Bottou, L., Bengio, Y., and Haffner, P. Gradient-based learning applied to document recognition. *Proceedings of the IEEE*, 86(11):2278–2324, 1998.
- Loshchilov, I. and Hutter, F. SGDR: Stochastic gradient descent with warm restarts. *International Conference on Learning Representations*, 2017.
- Lu, S. and Sengupta, A. Exploring the connection between binary and spiking neural networks. *Frontiers in Neuroscience*, 14:535, 2020.
- Orchard, G., Frady, E. P., Rubin, D. B. D., Sanborn, S., Shrestha, S. B., Sommer, F. T., and Davies, M. Efficient neuromorphic signal processing with loihi 2. In *2021 IEEE Workshop on Signal Processing Systems (SiPS)*, pp. 254–259. IEEE, 2021.
- Paszke, A. et al. Pytorch: An imperative style, high-performance deep learning library. *Advances in Neural Information Processing Systems*, 32:8026–8037, 2019.
- Patrick, L., Posch, C., and Delbruck, T. A 128×128 120 db 15μ s latency asynchronous temporal contrast vision sensor. *IEEE Journal of Solid-State Circuits*, 43:566–576, 2008.
- Perez-Nieves, N. and Goodman, D. F. Sparse spiking gradient descent. *arXiv preprint arXiv:2105.08810*, 2021.
- Perez-Nieves, N., Leung, V. C., Dragotti, P. L., and Goodman, D. F. Neural heterogeneity promotes robust learning. *Nature Communications*, 12(5791), 2021.
- Rahimi Azghadi, M., Chen, Y.-C., Eshraghian, J. K., Chen, J., Lin, C.-Y., Amirsoleimani, A., Mehonic, A., Kenyon, A. J., Fowler, B., Lee, J. C., et al. Complementary metal-oxide semiconductor and memristive hardware for neuromorphic computing. *Advanced Intelligent Systems*, 2(5): 1900189, 2020.
- Roy, K., Jaiswal, A., and Panda, P. Towards spike-based machine intelligence with neuromorphic computing. *Nature*, 575(7784):607–617, 2019.
- Rumelhart, D. E., Hinton, G. E., and Williams, R. J. Learning representations by back-propagating errors. *Nature*, 323(6088):533–536, 1986.
- Schaefer, C. J. and Joshi, S. Quantizing spiking neural networks with integers. In *International Conference on Neuromorphic Systems 2020*, pp. 1–8, 2020.
- Shaban, A., Bezugam, S. S., and Suri, M. An adaptive threshold neuron for recurrent spiking neural networks with nanodevice hardware implementation. *Nature Communications*, 12(1):1–11, 2021.
- Shrestha, S. B. and Orchard, G. SLAYER: Spike layer error reassignment in time. In *Proceedings of the 32nd International Conference on Neural Information Processing Systems*, pp. 1419–1428, 2018.
- Voelker, A. R., Rasmussen, D., and Eliasmith, C. A spike in performance: Training hybrid-spiking neural networks with quantized activation functions. *arXiv preprint arXiv:2002.03553*, 2020.
- Werbos, P. J. Backpropagation through time: What it does and how to do it. *Proceedings of the IEEE*, 78(10):1550–1560, 1990.
- Xiao, H., Rasul, K., and Vollgraf, R. Fashion-MNIST: A novel image dataset for benchmarking machine learning algorithms. *arXiv preprint arXiv:1708.07747*, 2017.
- Xu, Y., Zeng, X., Han, L., and Yang, J. A supervised multi-spike learning algorithm based on gradient descent for spiking neural networks. *Neural Networks*, 43:99–113, 2013.
- Zenke, F. and Vogels, T. P. The remarkable robustness of surrogate gradient learning for instilling complex function in spiking neural networks. *Neural Computation*, 33(4): 899–925, 2021.
- Zhang, W. and Linden, D. J. The other side of the engram: experience-driven changes in neuronal intrinsic excitability. *Nature Reviews Neuroscience*, 4(11):885–900, 2003.

A. Spiking Neuron Model

The dynamics of the passive membrane modeled using an RC circuit can be represented as:

$$\tau_m \frac{du_t}{dt} = -u_t + i_t r \quad (9)$$

where u_t is the hidden state (membrane potential) of the neuron at time t , $\tau_m = rc$ is the time constant of the membrane, r and c are the resistance and capacitance of the membrane, respectively, and i_t is the input current injection at time t .

The goal is to convert Equation (9) into a recurrent representation with fewer hyperparameters to enable training using backprop through time. The forward Euler method is used to find an approximate solution to Equation (9) without taking the limit $\Delta t \rightarrow 0$:

$$\tau_m \frac{u_{t+\Delta t} - u_t}{\Delta t} = -u_t + i_t r \quad (10)$$

For sufficiently small Δt , this provides a reasonable approximation of continuous-time integration. Isolating $u_{t+\Delta t}$ gives:

$$u_{t+\Delta t} = \left(1 - \frac{\Delta t}{\tau_m}\right)u_t + \frac{\Delta t}{\tau_m}i_t r \quad (11)$$

The change of u_t from one time step to the next can be found in absence of input current:

$$\beta = \frac{u_{t+\Delta t}}{u_t} = \left(1 - \frac{\Delta t}{\tau_m}\right) \quad (12)$$

To reduce the number of free variables in Equation (11), normalize $\Delta t = 1$, and let $r = 1\Omega$:

$$u_{t+1} = \beta u_t + (1 - \beta)i_t \quad (13)$$

To further simplify the model, let the effect of $(1 - \beta)i_t$ be approximated by a learnable weight scaled by the output of the previous layer, $(1 - \beta)i_t \leftarrow \sum_i w^{ij} z_t^i$. For computational efficiency (i.e., to enable inputs to be directly propagated from the input to the output of the network without delay), a time-shift is applied to z_t^i :

$$u_{t+1}^j = \beta u_t^j + \sum_i w^{ij} z_{t+1}^i \quad (14)$$

Finally, the term $-z_t^j \theta$ is added to Equation (14) to account for the neuronal reset mechanism where the threshold is subtracted from the membrane potential each time a spike $z_t^j = 1$ occurs:

$$u_{t+1}^j = \beta u_t^j + \sum_i w^{ij} z_{t+1}^i - \theta z_t^j. \quad (15)$$

B. Threshold Annealing Algorithm

Algorithm 2 Threshold Annealing: Same as Algorithm 1, but with temporal iteration decoupled from minibatch iteration

Require: $\theta_0 \in \mathbb{R}_{>0}$: Initial threshold

Require: $\theta_\infty \in \mathbb{R}_{>\theta_0}$: Final threshold

Require: $\alpha_\theta \in \mathbb{R}_{>0}$: Inverse threshold time constant

Require: w : Initial parameters

Require: η : Learning rate

$\theta_\gamma \leftarrow \theta_0$ (Initialize threshold)

$s \leftarrow \partial \tilde{z}(\theta_0) / \partial u$ (Initialize surrogate gradient using θ_0)

$\gamma \leftarrow 0$ (Initialize training step)

while w not converged **do**

$\gamma \leftarrow \gamma + 1$

for $t \in \{1, \dots, N\}$ **do**

$\mathcal{L} \leftarrow f(w_{\gamma-1}, \theta_\gamma)$ (Get loss by iterating through N time-steps during forward-pass)

$g_\gamma \leftarrow \nabla_w \mathcal{L}$ (Get gradients w.r.t. surrogate gradient s using initial threshold θ_0)

end for

$w_\gamma \leftarrow w_{\gamma-1} - \eta \cdot g_\gamma$ (Update parameters e.g. using SGD or Adam)

$\theta_\gamma \leftarrow \theta_{\gamma-1} + \alpha(\theta_\infty - \theta_{\gamma-1})$ (Update threshold *outside* of forward-pass temporal loop, without updating s)

end while

return: w_γ (Resulting parameters)

Algorithm 2 is a more detailed form of Algorithm 1 to highlight how the temporal-loop during the forward-pass is decoupled from the minibatch training loop. Homeostasis would place the threshold update θ_γ within the for-loop to stabilize neuronal activity, whereas threshold annealing takes it out to increase the effective hidden state precision whilst reducing both memory and computational complexity.

C. Upper Bound on the Rate of Threshold Annealing

To minimize the impact threshold updates have on a network's ability to learn, we set the constraint that the threshold update cannot exceed the weight update-induced membrane potential change. Formally, the threshold update $\Delta\theta_\gamma = \theta_{\gamma+1} - \theta_\gamma$ is bounded by how far the new membrane potential at $\gamma + 1$ is from the original threshold at γ :

$$\Delta\theta_\gamma < u_{\gamma+1} - \theta_\gamma \quad (16)$$

For simplicity, we assume this takes place at the first spike time for an instantaneous input (which is why notation for time t has been dropped), though this constraint will be relaxed. $\Delta\theta_\gamma = \theta_{\gamma+1} - \theta_\gamma$ can be found from Equation (4):

$$\Delta\theta_\gamma = \alpha(\theta_\infty - \theta_\gamma) \quad (17)$$

which is substituted into Equation (16):

$$\alpha(\theta_\infty - \theta_\gamma) < u_{\gamma+1} - \theta_\gamma \quad (18)$$

Considering only one spiking neuron, the immediate post-synaptic current influence at the spike time from Equation (1) for iterations γ and $\gamma + 1$ is given below:

$$u_\gamma = \mathbf{z} \cdot \mathbf{w}_\gamma^{:j} \quad (19)$$

$$u_{\gamma+1} = \mathbf{z} \cdot \mathbf{w}_{\gamma+1}^{:j} \quad (20)$$

where $\mathbf{z} \in \mathbb{R}^i$ is the input vector, $\mathbf{w}_\gamma^{::j} \in \mathbb{R}^i$ is the weight vector connected to the j^{th} neuron of the first layer (and can be generalized to subsequent layers). For simplicity, assume the weight update is calculated via stochastic gradient descent (SGD), though noting that the final term below should be substituted for the preferred optimization update rule:

$$\mathbf{w}_{\gamma+1}^{::j} = \mathbf{w}_\gamma^{::j} + \eta \frac{\partial \mathcal{L}}{\partial \mathbf{w}_\gamma^{::j}} \quad (21)$$

Equation (21) is substituted back into Equation (20):

$$u_{\gamma+1} = \mathbf{z} \cdot \left(\mathbf{w}_\gamma^{::j} + \eta \frac{\partial \mathcal{L}}{\partial \mathbf{w}_\gamma^{::j}} \right) \quad (22)$$

which is then substituted into Equation (18):

$$\alpha(\theta_\infty - \theta_\gamma) < \mathbf{z} \cdot \left(\mathbf{w}_\gamma^{::j} + \eta \frac{\partial \mathcal{L}}{\partial \mathbf{w}_\gamma^{::j}} \right) - \theta_\gamma \quad (23)$$

$$\implies \underbrace{(1 - \alpha)\theta_\gamma}_{\text{const.}} + \underbrace{\alpha\theta_\infty}_{\text{const.}} < \underbrace{\mathbf{z}}_{\text{const.}} \cdot \left(\mathbf{w}_\gamma^{::j} + \underbrace{\eta \frac{\partial \mathcal{L}}{\partial \mathbf{w}_\gamma^{::j}}}_{\text{update}} \right) \quad (24)$$

All constant terms have been underlined, and the evolution of $\mathbf{w}_\gamma^{::j}$ is dependent on $\partial \mathcal{L} / \partial \mathbf{w}_\gamma^{::j}$. When using more common optimizers, such as Adam or SGD with momentum, the weight update term must be swapped out. For the Adam optimizer, the update term will follow an exponential decay as the network approaches training convergence until the right hand side of Equation (24) stabilizes at $\mathbf{z} \cdot \mathbf{w}_\gamma^{::j}$. The only reasonable and valid solution as $\gamma \rightarrow \infty$ is for θ_γ to exponentially relax to θ_∞ , where the update term approaches zero where adaptive/exponential decay is applied, and the term on the left factors out to:

$$\theta_\infty < \mathbf{z} \cdot \mathbf{w}_\infty^{::j} \quad (25)$$

θ_γ and θ_∞ taking on values much less than the dot product of the input and weights would be a mathematically valid solution, but at the cost of each neuron no longer having a sufficiently wide state-space and the ability to trigger spikes (see Section 2.2 for detail on why memory and spike emission become mutually exclusive as the threshold is reduced). Therefore, an exponential relaxation to a steady-state threshold described in Equation (3) is the optimal solution for exponentially adaptive weight decays.

Furthermore, \mathbf{z} is a time-varying input (it is only constant across iterations given it represents the same input data), and so Equation (25) must be generalized to account for the historical contributions of post-synaptic current to the membrane state at the spike time (Equation (1)).

The above conditions were derived assuming that the threshold update should not impact spiking activity at all, which is unnecessarily stringent. As long as each neuron fires at least once, then the immediate weights attached to its input will contribute to the output loss, have a gradient signal (for dense layers), and therefore avoid becoming dead neurons. A more reasonable objective would be to only introduce the constraint from Equation (25) when a neuron is emitting at most a single spike across the simulation run time.

D. Experimental Results

Parameter Initialization: For all experiments, parameters were initialized using the default methods in PyTorch 1.10.1. Dense layers were initialized by uniformly sampling from $U(-\sqrt{a}, \sqrt{a})$:

$$a = \frac{1}{N_{\text{in}}}, \quad (26)$$

where N_{in} is the number of input features. Convolutional layer parameters were also uniformly sampled:

$$a = \frac{1}{C_{\text{in}}N_xN_y} \quad (27)$$

where C_{in} is the number of input channels, and N_x and N_y are the kernel dimensions.

Hyperparameter search: The following hyperparameters were searched in all experiments:

- β : neuron decay rate/membrane potential inverse time constant (Equation (1))
- θ : firing threshold (Equation (2))
- k : surrogate gradient slope (Equation (8))
- η : initial learning rate
- **GC**: gradient clipping
- **WC**: weight clipping
- **DO**: dropout rate (dense layers)
- **BN**: batch normalization (convolutional layers)

The following hyperparameters were searched in all threshold annealing experiments:

- θ_0^L : initial firing threshold of all neurons in layer L (Equation (4))
- θ_∞^L : final firing threshold of all neurons in layer L (Equation (4))
- α^L : inverse time constant of threshold of all neurons in layer L (Equation (4))

Hyperparameters were selected based on 500 separate trials for each experiment using a tree-structured Parzen Estimator algorithm to randomly sample from the search space in Optuna (Akiba et al., 2019; Bergstra et al., 2011). Based on this approach, individual hyperparameters were found for high precision, BSNN, BSNN with normalized threshold, and BSNN with threshold annealing across all four datasets. I.e., 16 different sets of hyperparameters were found.

With respect to the threshold:

- High precision and BSNN experiments set the threshold as a free hyperparameter,
- BSNN with normalized threshold fixes the threshold at $\theta = 1$, and
- BSNN with threshold annealing set the initial threshold θ_0 , final threshold θ_∞ , and inverse time constant α as free hyperparameters.

Due to the additional hyperparameters in the BSNN with threshold annealing experiment, the final result would likely benefit from using additional trials during the hyperparameter search. But for fairness, this was fixed to 500 trials as with all other cases.

Optimization: Unless otherwise specified, the Adam optimizer was used with 1st and 2nd order moment estimates set to $(\beta_1, \beta_2) = (0.9, 0.999)$. A cosine annealed learning rate with warm restarts is computed using the following scheduler (Loshchilov & Hutter, 2017; He et al., 2019):

$$\eta_t = \frac{1}{2}\eta\left(1 + \cos\left(\frac{\pi\gamma}{T}\right)\right), \quad (28)$$

where η is the initial learning rate, γ is the iteration, and T is the period of the schedule. For all cases where cosine annealing is used, T is set to a period of 10 training epochs.

The fast sigmoid surrogate gradient was used for all spiking neurons (Equation (8)).

D.1. Temporal Coding

A corresponding notebook to replicate these experiments, in addition to animated visualizations of the threshold evolution and its impact on membrane potential, are provided in the source code.

Architecture: A 3-layer fully connected network was used with 100–1000–1 neurons.

Hyperparameters: The hyperparameters of the temporal coding task from Section 4.1 are shown in the table below, and were chosen arbitrarily for the sake of an intuitive demonstration of threshold annealing.

Table 3. Hyperparameters for Temporal Coding Task

Precision	β	θ	θ_0	θ_∞	α	k	η
flt32	0.6	2.0	–	–	–	5.0	1e-3
BSNN; $\theta=1$	0.15	1.0	–	–	–	5.0	1e-3
BSNN; $\theta=50$	0.15	50.0	–	–	–	5.0	1e-3
Proposed	0.15	–	5.0	50.0	5e-3	5.0	1e-3

¹ Stochastic Gradient Descent with momentum of 0.9 was used for all temporal coding experiments. No schedule was used.

Loss: Let y_t be the target membrane potential of the output neuron at time t . The total mean square error is calculated by summing the loss across all time steps T :

$$\mathcal{L}_{MSE} = \sum_t^T (y_t - u_t)^2. \quad (29)$$

Peak membrane target: The peak of the target membrane potential in Figure 4 is set to be 10% above the threshold to increase the probability of spike emission.

D.2. Static Datasets

Hyperparameters: The hyperparameters used in the static dataset experiments from Section 4.2 are shown in the table below.

Table 4. Hyperparameters for Static Datasets

Dataset	Precision	β	θ	k	η	GC	WC	BN	DO
MNIST	flt32	0.92	2.0	6.0	1.9e-3	✓	✓	✓	0.09
MNIST	BSNN; θ :1	0.74	1.0	4.7	6.5e-3	✗	✗	✓	0.87
MNIST	BSNN	0.84	6.4	2.8	2.7e-3	✗	✗	✓	0.06
MNIST	Proposed	0.99	—	10.2	1.0e-2	✗	✗	✓	0.03
FMNIST	flt32	0.39	1.5	7.7	2.0e-3	✓	✓	✓	0.13
FMNIST	BSNN; θ :1	0.82	1.0	4.3	1.2e-3	✓	✓	✓	0.86
FMNIST	BSNN	0.87	9.7	6.7	1.6e-2	✓	✗	✓	0.01
FMNIST	Proposed	0.87	—	0.2	8.4e-4	✗	✗	✓	0.65

¹ 16Conv5-AP2-64Conv5-AP2-1024Dense10.

² Batch size of 128 used for all experiments.

³ MNIST flt32 did not use a learning rate schedule.

⁴ FMNIST Proposed used SGD with momentum set to 0.86.

Table 5. Threshold Annealing Hyperparameters for Static Datasets

Dataset	θ_0^1	θ_∞^1	α^1	θ_0^2	θ_∞^2	α^2	θ_0^3	θ_∞^3	α^3
MNIST	11.7	16.0	2.4e-2	14.1	30.4	0.12	0.7	4.2	1.1e-3
FMNIST	6.9	14.0	3.7e-2	10.3	23.1	0.30	18.0	27.9	0.10

¹ θ_0^L is the initial threshold of all neurons in layer L .

² θ_∞^L is the final threshold of all neurons in layer L .

³ α^L is the inverse time constant of the threshold for all neurons in layer L .

Loss: To emulate the limitations of efficient neuromorphic hardware, we assume the membrane potential is an inaccessible hidden state when calculating the loss function (Azghadi et al., 2020). Instead, we train our network under the more challenging constraint of using target spike counts for each class. The spikes of each output neuron z_t^j are accumulated over time. The mean square error loss of the target count c^j is calculated and then summed across the N output classes ($N = 10$).

Let y_t be the target membrane potential of the output neuron at time t . The total mean square error is calculated by summing the loss across all time steps T . We follow a similar approach to SLAYER (Shrestha & Orchard, 2018) where the target of the correct class c is to fire 80% of the time, and incorrect classes are set to fire 20% of the time to avoid excessive suppression of neuronal activity:

$$\mathcal{L}_{MSE} = \sum_j^N \sum_t (c^j - z_t^j)^2. \quad (30)$$

D.3. Temporal Datasets

Hyperparameters: The hyperparameters used in the temporal dataset experiments from Section 4.3 are shown in the table below.

Table 6. Hyperparameters for Temporal Datasets

Dataset	Precision	β	θ	k	η	GC	WC	BN	DO ¹	DO ²
DVS128	flt32	0.72	2.5	5.4	7.5e-3	✗	✓	✓	0.29	–
DVS128	BSNN; θ :1	0.1	1.0	0.1	3.6e-3	✗	✗	✗	0.64	–
DVS128	BSNN	0.78	8.7	0.3	9.6e-4	✓	✓	✗	0.06	–
DVS128	Proposed	0.93	–	0.2	1.8e-3	✓	✗	✗	0.43	–
SHD	flt32	0.98	1.7	2.0	2.7e-4	✗	✗	–	0.05	0.04
SHD	BSNN; θ :1	0.61	1.0	0.4	1.9e-4	✓	✓	–	0.09	0.11
SHD	BSNN	0.33	3.4	0.1	5.0e-4	✓	✓	–	0.22	0.07
SHD	Proposed	0.95	–	0.3	6.5e-4	✓	✓	–	0.02	0.19

¹ DVS128: 16Conv5-AP2-32Conv5-AP2-800Dense11

² DVS128 flt32 batch size: 16. DVS128 BSNN batch size: 8.

³ DVS128 events integrated over 5 ms.

⁴ SHD: 700Dense3000Dense20

⁵ SHD batch size: 32

⁶ SHD flt32 events integrated over 2 ms; BSNN events integrated over 3 ms.

⁷ DO¹: dropout rate in the first dense layer, DO²: dropout rate in second dense layer

Table 7. Threshold Annealing Hyperparameters for Temporal Datasets

Dataset	θ_0^1	θ_∞^1	α^1	θ_0^2	θ_∞^2	α^2	θ_0^3	θ_∞^3	α^3
DVS128 Gesture	10.4	12.2	3.3e-3	16.6	19.1	6.1e-3	6.8	16.5	0.17
SHD	13.5	45.2	2.8e-5	11.2	51.1	1.36e-5	–	–	–

¹ θ_0^L is the initial threshold of all neurons in layer L .

² θ_∞^L is the final threshold of all neurons in layer L .

³ α^L is the inverse time constant of the threshold for all neurons in layer L .

Loss: For both networks, the same loss function is used as in Equation (30).

E. Discussion

E.1. Spike Activity on Static Datasets

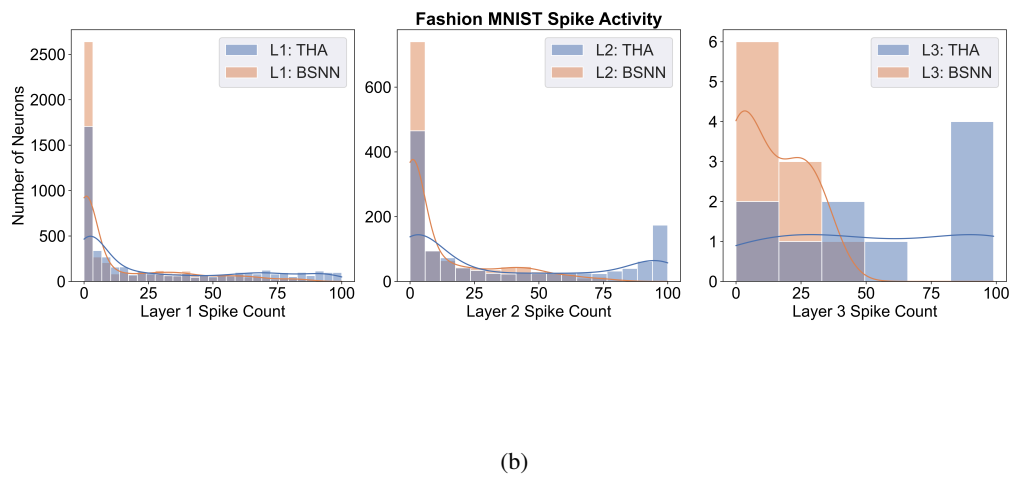
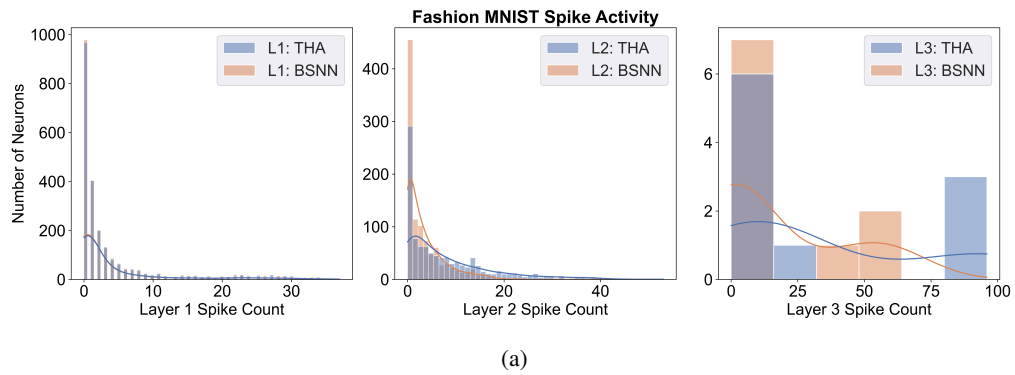


Figure 7. Spiking activity across layers at the start of the training process of BSNNs with threshold annealing (THA) and without (BSNN) on static datasets.